PCCP

ROYAL SOCIETY OF CHEMISTRY

PAPER

View Article Online
View Journal | View Issue

Cite this: *Phys. Chem. Chem. Phys.*, 2022, **24**, 12410

Adsorption properties of pyramidal superatomic molecules based on the structural framework of the Au_{20} cluster†

Qiman Liu, *[ab] Manli Zhang,[a] Dawen Zhang,[a] Yunhu Hu,[a] Qiyong Zhu*[a] and Longjiu Cheng *[b]

The pyramidal Au_{20} cluster is a highly inert and stable superatomic molecule, but it is not suitable as a potential catalyst for covalent bond activations, *e.g.*, CO oxidation reaction. Herein, the adsorption and electronic properties of CO molecules on various pyramidal clusters based on the structural framework of Au_{20} are investigated using density functional theory. According to the SVB model, we constructed isoelectronic superatomic molecules with different pyramid configurations by replacing the vertex atoms of the Au_{20} using metal M atoms (M = Li, Be, Ni, Cu, and Zn group atoms). After the CO molecules are adsorbed on the vertex atoms of these metal clusters, we analyzed the CO adsorption energies, C–O bond stretching frequencies, and electronic properties of the adsorption structures. It was found that the adsorption of CO molecules results in minimal changes in the parent geometries of the pyramidal clusters, and most adsorption structures are consistent with the geometry of CO adsorption at the vertex site of the Au_{20} cluster. There are significant red shifts when CO molecules are adsorbed on the Ni/Pd/Pt atoms of the clusters, and their CO adsorption energies were also greater. The molecular orbitals and density of states reveal that there are overlaps between the frontier orbitals of the clusters and CO, and the electronic structure of $NiAu_{19}^-$ is not sensitive to CO. The ETS-NOCV analysis shows that the increase in the density of the bonding area caused by the orbital interactions between the fragments is higher than the decrease in the density of the bonding area caused by Pauli repulsion, presenting that the direction of charge flow in the deformation density is from CO → clusters. From energy decomposition analysis (EDA) and NPA charge, we find a predominant covalent nature of the contributions in CO···M interactions (σ-donation). Our study indicates that the SVB model provides a new direction to expand the superatomic catalysts from the superatom clusters, which also provides inference for the extension of the single atom catalysis.

Received 4th April 2022,
Accepted 2nd May 2022

DOI: 10.1039/d2cp01552h

rsc.li/pccp

1. Introduction

Considering the global demands for new energy materials, improved methods to reduce pollution, advanced methods for the production of fine chemicals, sensors for detecting harmful substances, and new methods for evaluating medical and biological problems, it is clear that catalysis affects all of these, which are very basic subjects of scientific research.[1–6] Nowadays, numerous metal clusters are being studied with atomic accuracy, which have attracted widespread research interest recently in the search for significant catalytic reactions with high catalytic activities and unique selectivity.[1,4–8] After the earlier findings that Au clusters have fantastic activities for CO oxidation reactions, several studies have been dedicated to reveal catalytic/adsorption reactions of O_2 and CO molecules on Au clusters that are isolated in the gas phases or supported on the surfaces of metallic oxides.[9–15] Gold clusters that show propensity for O_2 adsorption can also adsorb CO molecules at the same time, thus indicating them as possible catalyst models for the CO oxidation reactions.[10,16–18] Among them, the chemisorption and dissociation of gas molecules on the gold surfaces are the focus.[11,18–20] It has been confirmed that CO molecules have a propensity to be adsorbed on low-coordinated gold atoms, where the carbon atoms bind to Au atoms at the peripheries of the clusters.[21–23] For example, Zhai and Wang found strong chemisorption of few CO molecules on

[a] *School of Chemistry and Materials Engineering, Huainan Normal University, Huainan, 232038, P. R. China. E-mail: qimliu@ustc.edu.cn, zhuqiyong2651@163.com*

[b] *Key Laboratory of Structure and Functional Regulation of Hybrid Materials, Anhui University, Ministry of Education, Hefei, 230601, P. R. China. E-mail: clj@ustc.edu.cn*

† Electronic supplementary information (ESI) available. See DOI: https://doi.org/10.1039/d2cp01552h

top of low-coordinated atoms in anions of Au clusters using photoelectron spectroscopy combined with density functional theory (DFT).[24] Lopez *et al.* attributed the origins of catalytic activities to the abundances of low-coordinated Au on the cluster surfaces and interactions between the clusters and substrates.[25]

Structures of metal clusters are critical for investigating molecular adsorption. Interestingly, the naked neutral Au_{20} tetrahedral cluster, which showed high stability in the gas phase, is like a fragment of the fcc (face-centered cubic) bulk gold, which was verified by photoelectron spectroscopy and theoretical calculations.[26] Cheng *et al.* suggested that Au_{20} can be considered as a superatomic molecule using chemical bonding analyses, where a molecule-like electronic structure of the pyramidal cluster is achieved by four D_3S hybridization orbits of superatomic Au_{16} bonding with four vertical Au atoms.[27] Recently, this system was reanalyzed by Muñoz-Castro *et al.* Their computation results indicated that Au_{20} was described as the integration of concentric structures, which is depicted by Au_{16}–Au_4 with a considerable sharing of the electron densities between the different concentric structures, where the superatomic Au_{16} core shares electron density with the four capping gold atoms, further verifying that the tetrahedral cluster is a superatomic molecule.[28] Such magic configuration makes all gold atoms appear on the surface of the cluster, where each of four triangular planes of the tetrahedron represents a (111) lattice surface of the bulk Au solids with different coordination environments (adsorption sites, involving edge, inner, and vertex).[21,29–33]

Atomically precise clusters should be ideal catalyst models because they have well-defined structures and uncoordinated surface sites as the active centers. Fortunately, the pyramidal Au_{20} cluster provides a unique opportunity for such ideal model systems. However, it was well known that the Au_{20} cluster only has weak interactions with CO molecules and hardly interacts with O_2.[21] The presence of other metal atoms in gold clusters provide convenient opportunities to modulate the geometric and electronic characteristics of corresponding Au-based clusters. Consequently, their reactive activations can be altered in desirable manners. For example, the icosahedral $Au_{12}Ag$ cluster showed enhancement in CO adsorption in comparison to that of the pure gold cluster.[34] The presence of alkali metal atoms such as Li and Na, as well as transition atoms such as Ti, V, Pd, and Pt can dramatically enhance the chemical reactivity of the parent Au clusters toward the adsorption of CO and O_2 molecules.[7,35–37] Tapan reported a systematic research on the structural properties of one Li atom substitution in Au_{20} and found that Li substitution generates a noteworthy increase in the adsorption energy of the CO molecule in $Au_{19}Li$ than that of pyramidal Au_{20}.[32] Subsequently, they also reported that the low coordinated vertex-Pt atom site of $Au_{19}Pt$ clusters is much more reactive than Au atom sites.[38]

There are some specific clusters, termed as superatoms, which can mimic the chemical behaviors of single atoms or a group elements in the periodic table of elements.[39–41] In fact, the existing idea of the theory depends on achieving stabilities through the electronic shell closures of paired electrons. A well-known example of Al_{13}, with 39 valence electrons, needs one extra electron to close the $2p^6$ shells and behave as a halogen atom.[42] The concept of superatomic molecules (SVB model) proposed by Cheng and Yang is a quite recent and interesting field that has been highly successful in understanding the stability of clusters and interactions between superatoms.[43] In this model, superatoms could form delocalized super bonds by sharing both valence pairs and nuclei with other superatoms or atoms, which gives new insights into the structures of non-spherical clusters.

Adsorption is the basic behavior of the interface. This process has an impact on the atomic structure, electronic structure, catalysis/photoelectric, and other properties of the interface; thus, it is a very basic and important problem. Moreover, the SVB model provides a new direction to expand the superatomic catalyst from superatom clusters, which can be used as an extension of single atom catalysis. Hence, the adsorption properties of CO molecules on various pyramidal clusters based on the structural framework of Au_{20} were investigated using DFT. According to the SVB model, we construct isoelectronic superatomic molecules with different pyramid configurations by replacing the vertex atoms of the pyramidal Au_{20} using different metal M atoms (M = Li, Be, Ni, Cu, and Zn group atoms). After CO molecules are adsorbed on the vertex atoms of these metal clusters, the CO adsorption energies, C–O stretching frequencies, geometries, and electronic properties of adsorption structures are analyzed.

2. Computational methods and details

The optimization of the cluster structures and their subsequent calculations was carried out using the non-empirical hybrid GGA functional PBE0 level of theory with the Def2-TZVP basis set.[44,45] The basis set is used in connection with the relativistic effective core potential for heavy metal atoms. The structure energies of pyramidal clusters reported herein considered the contributions of zero-point energy (ZPE) corrections. The vibrational frequencies were verified to guarantee that our structures belong to the true local minima at the same theoretical level. The calculations of the electrostatic potential $V(r)$ are performed to analyze the distributions of atom charges on the surfaces of the clusters, and these methods are rigorously defined from the ref. 46. All computations are realized using the GAUSSIAN 09 package.[47] The visualizations of the molecular orbitals (MOs) are performed based on the MOLEKEL 5.4 program.[48] The energy decomposition analysis (EDA) from the symmetry-adapted perturbation theory (SAPT) is performed using the Psi4 package, and the lowest-order expansion in the SAPT is given by SAPT0.[49,50]

3. Results and discussion

3.1 Adsorption properties of pyramidal Au_{20} clusters

Our optimized Au_{20} structure agrees with previous works.[26,28] Based on the SVB model, it has been confirmed that the cluster

can be viewed as a super CH_4 molecule analogue in the bonding framework. In fact, removing any one of its four external Au atoms, the remaining Au_{19} is in C_{3v} symmetry and exposes a bonding site. Here, it is very important to mention that the globally minimal structure of the neutral Au_{19} cluster has been reported to be a truncated pyramid.[51] Moreover, earlier, Fielicke and coworkers found that the reduction in the symmetry when a vertex Au atom is removed from the tetrahedral Au_{20} cluster can be directly characterized in the vibrational spectrum of Au_{19}.[52] The electrostatic potential surface $V(r)$ of the Au_{20} cluster (Fig. 1a) shows that four vertex Au atoms have positive charge excesses with four significant σ-hole regions, while the negative charge excesses are distributed in other gold atoms. These results indicate that vertex Au atoms are active sites for both charge-controlled and frontier-controlled interactions with some electron donors, *e.g.*, CO and NH_3 molecules. For instance, the negatively charged site of C atom in the CO molecule adsorbs at the vertex Au atoms for the subsequent formation of adducts by electrostatic interactions.

To obtain the initial adsorption structures of the cluster-CO complexes, we placed a single CO molecule in various sorts of nonequivalent positions of pyramidal Au_{20}, involving the top, hollow, and bridge sites. However, we found that most adsorption geometries have imaginary frequencies or cannot converge to stable structures. The three stable structures of the Au_{20}–CO complexes with the singlet state are shown in Fig. 1b, and the detailed information on the interactions of the CO molecule with the vertex and edge and surface Au atoms (*v*-site, *e*-site, and *s*-site isomers). The *v*-site isomer is the global minimum. It can be seen that the adsorption of the CO molecule generates minimal changes in the parent structure of Au_{20}. Computed CO and Au–CO bond distances (r), vibrational frequencies (ν), and adsorption energies (E_{ae}) of the Au_{20}–CO complexe are listed in Table 1. The E_{ae} values are given by the following equation: $E_{Au_{20}-CO} - E_{Au_{20}} - E_{CO}$. From this table, we observe that the C–O distances and vibrational frequencies of the adsorption structures have very slight changes than that of the free CO molecule because the 5*d* lone pair electrons of the Au atoms of

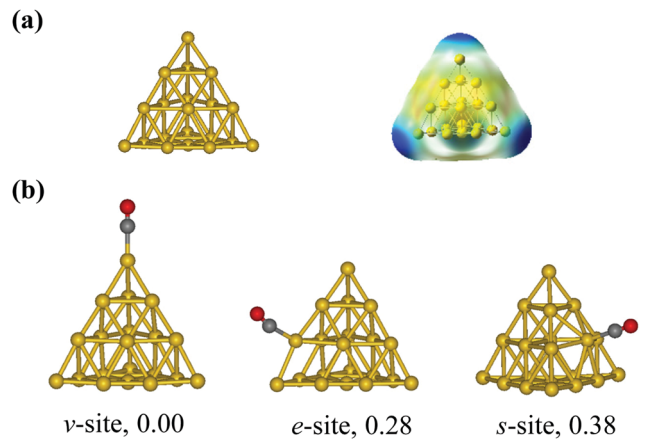

Fig. 1 (a) The optimized structure and electrostatic potential surface of the Au_{20} cluster. (b) Selected optimized geometries of the pyramidal Au_{20}–CO system. Labeled are the energies (eV) relative to the global minimum.

Table 1 Bond length (r, Å), bond stretching frequencies (ν, cm^{-1}), and E_{ae} (eV) values for the Au_{20}–CO complexes

Sites	r(C–O)	r(Au–C)	ν(C–O)	ν(Au–C)	E_{ae}
v-site	1.125	2.00	2217.15	326.29	0.69
e-site	1.127	2.04	2186.08	291.38	0.48
s-site	1.126	2.02	2205.33	281.62	0.53

the Au_{20} delocalize toward the antibonding π-orbitals of the CO molecule. However, it is clear that the pyramidal Au_{20} has very weak interactions with CO, where the interactions of the σ-donation coordinations contributed to values of E_{ae}. Overall, Au_{20} is a highly inert and stable molecule, but it is not suitable as a potential catalyst for covalent bond activation.

3.2 Adsorption characters of pyramidal superatomic molecules

Although gas molecules (*e.g.*, CO and O_2) weakly interact with the free Au_{20} cluster and are not very effective in putting into practice CO gas oxidation, it has been confirmed that low-coordinated Au sites on the surface of the pyramidal cluster play a prominent role in many other catalytic reactions. The most active sites (vertex sites) for the Au_{20} superatom have been identified, thus enlightening the rational design of pyramidal nanostructures with special sites based on the structural framework of Au_{20}. It is well known that the chemical activity of the Au clusters can be tuned by the way of doping another atom. Here, our purpose is to study the effects of local environments on CO adsorption; thus, the adsorption of doped structures is only studied on the top Au sites. Compared to the pure Au_{20} cluster, metal clusters with two types of atoms have very uneven charge distributions by the doping strategy, resulting in the formation of different Lewis acid and Lewis base sites that can make clusters reactive.

As mentioned before, the vertex sites of the Au_{20} cluster have been confirmed to be an excellent model for studying the adsorption behaviors of CO molecules compared to the Au atoms at other sites. Our main purpose is to construct isoelectronic superatomic molecules in pyramid configurations according to the guidance of the SVB theory. Hence, we need to know the correct geometric structures of these systems. We retrieved the relevant literatures and the periodic table of elements to find other metal atoms that have isoelectrons with the Au atom. The calculations of the response properties are carried out by employing the optimized structures of the $Au_{19}M$ clusters where the structures are generated from the tetrahedral geometry of the Au_{20} cluster by replacing one vertex Au atom by other metal M atoms (M = Li, Be, Ni, Cu, and Zn groups). Vibration frequencies analyses indicated that all the optimized structures indeed correspond to real local minima on the potential energy surfaces. These pyramidal structures of the 20e $Au_{19}M$ clusters satisfy the magic numbers of the SVB model.

To get the initial adsorption structures of $[Au_{19}M]$–CO, we placed a single CO molecule in the vertex sites of the pyramidal frameworks. All adsorption structures of the Au_{19}–M clusters with CO molecules are then optimized at the theoretical level of

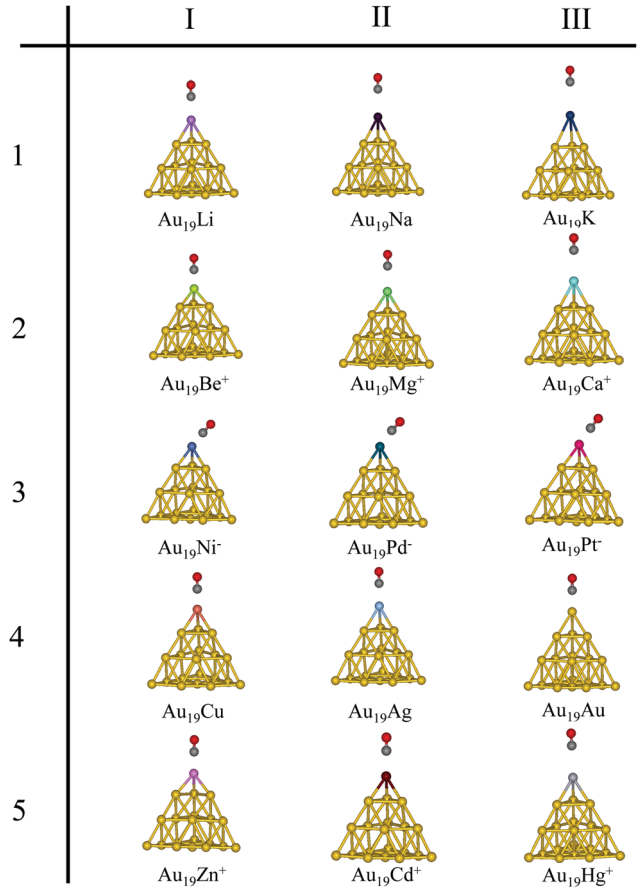

Fig. 2 Optimized geometries for activated CO complexes with pyramidal structures.

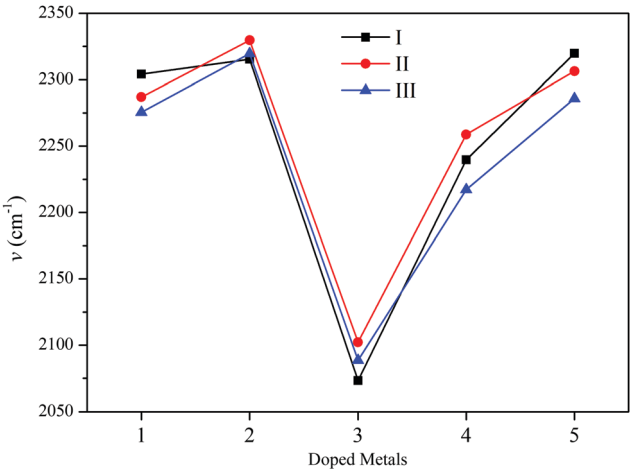

Fig. 3 Schematic comparisons of C–O vibration frequencies of the adsorption structures.

PBE0/Def2-TZVP for different spin multiplicities (singlet and triplet) to find the spin multiplicities of the ground states. After geometry optimizations, we also calculated their vibrational frequencies to verify the stabilities. The geometries of CO-adsorbed Au_{19}–M clusters that are identified for the singlet spin states are displayed in Fig. 2. We can also find that the adsorption of CO molecules causes very minimal changes in the parent structures, due to which these superatomic molecules have very high electronic stabilities. Among them, most adsorption structures are consistent with the geometry structure of CO adsorption at the vertex site of the Au_{20} cluster. In comparison, there are significant shifts when CO molecule is adsorbed on the Ni group atoms. In brief, the adsorbed Li, Be, and Zn group atoms have linear (perpendicular) geometries, while Ni group atoms change to bent geometries as a result of the strong C–Ni interaction. Moreover, we found that metal atoms with different atomic radii have no obvious effects on the alloy clusters maintaining the pyramid configurations. In general, only judging from the geometric structures are the results we want.

Fig. 3 showed the C–O stretching frequencies of the adsorption structures. In these complexes, the vibrational frequencies of the CO molecules are quite different from that of free CO (2239.79 cm^{-1}). As we know, the vertex Li, Be, and Zn group atoms contributed *s* valence-shell electrons to the pyramid structures, allowing them to satisfy the stable electronic structures of the superatomic molecule model. These metals typically engage in chemical bonding through their n*s* valence orbitals, where n is the principal quantum number. When the CO molecule binds to these vertex metal atoms, the major interactions are the σ-donation coordination from the 5*s* orbital of the CO molecule to the empty valence orbitals of the alloy clusters, and the *p*-π conjugated interaction leads to their vibrational frequencies in the 1, 2, and 5 rows showing very significant increases. However, the situations in the Ni group atoms are very different. For example, the CO vibration frequency of the $[NiAu_{19}^{-}]$–CO (2073.39 cm^{-1}) is less than that of the free CO. This is because that 5*d* lone pair electrons of the Ni atom of the superatom molecule delocalize toward the antibonding π orbitals of the CO molecule. Overall, the σ-donation of the electron density from CO to the metal and π-back-donation from the metal to CO takes place. These situations have been also summarized in previous works.[53–55] For example, Professor Johnston' team elaborated on the influence of Pd-doping on the interactions between CO molecules and small cationic gold clusters.[53] Other molecules with multiple bonds (*e.g.*, CN and N_2) are adsorbed on the vertex sites of these pyramidal clusters, and N–N bond lengths are also slightly elongated, while C–N bond lengths are in accordance with isolated CN (Fig. S1, ESI†).

The E_{ae} values measure the magnitude of the adsorption energies of the CO molecules to the metal clusters, and are given by the following equation: $E_{ae} = E_{cluster\ -\ CO} - E_{cluster} - E_{CO}$, where $E_{cluster-CO}$ is the total energy of the adsorbed systems, while $E_{cluster}$ and E_{CO} are the total energies of the clusters and the isolated CO molecule, respectively. The calculated results for the E_{ae} values are shown in Fig. 4, and it can be seen from this figure that the results for E_{ae} values match quite well with those of the frequency analyses of the previous paragraph. The E_{ae} values of CO molecules that bind with the Li and Zn group atoms are relatively small (<0.5 eV),

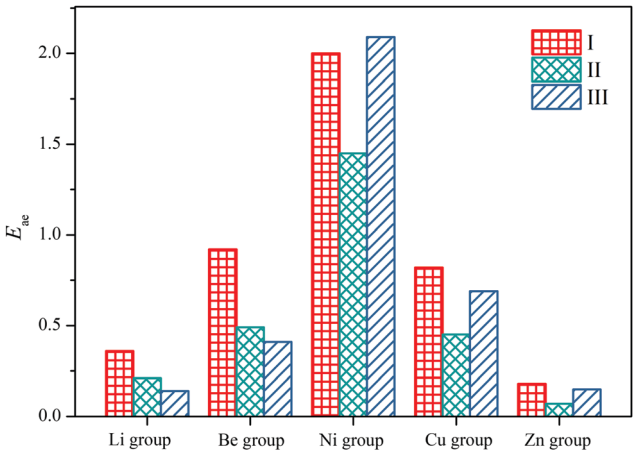

Fig. 4 Schematic comparisons of the calculated adsorption energies for the CO on M atoms of pyramidal superatomic molecules (M = Li, Be, Ni, Cu, and Zn groups).

and the E_{ae} values of CO–Be are in the range of (0.5–1.0) eV. It is surprising that the E_{ae} values of the CO molecules that bind with Ni group atoms are in the range of 1.5–2.0 eV, which are in the category of the covalent bond. Moreover, we found that the E_{ae} values are independent of the atomic radii of the M atoms (M = Li, Be, Ni, Cu, and Zn groups).

The thermal stabilities of the selected adsorption structures are were carried out using the *ab initio* molecular dynamics (AIMD) simulations.[56–59] The simulations lasted for 10 ps with a time step of 2.0 fs at initial temperatures of 300 K and 500 K, respectively. Snapshots were extracted every 20 fs for demonstration and the snapshots after a 10 ps AIMD simulation are plotted. Details for the AIMD simulations are shown in Fig. S2 (ESI†). It can be observed that the adsorption structures maintain integrity at a temperature of 500 K, suggesting their good thermal stabilities in a high temperature environment.

3.3 Electronic properties of the adsorption structures

The pyramidal 20e metal clusters have molecule-like electronic structures, and the SVB model clearly describes their high electronic stabilities, which can be seen in the many references. Through heteronuclear metal atom doping, the original charge distributions are still broken even though the structural framework of the parent Au_{20} is retained, and the obtained cluster structures form new adsorption sites. For these systems, CO adsorption is very weak on metal atoms with *s* valence-shell electrons, but it is very strong on the vertex Ni group atoms. More importantly, for the research scopes of the present paper, the SVB model is used as a theoretical guidance to search for novel catalytic sites, meaning that the pyramidal clusters need maintain to the integrities of their own electronic properties. It is natural to try to explore why the CO adsorption energies of metal clusters vary with different compositions, and to determine whether there are correlations between the valence-shell electrons and adsorption energies. In order to get deeper insights into the electronic properties that play a role in the adsorption of CO molecule, we analyzed the molecular orbitals

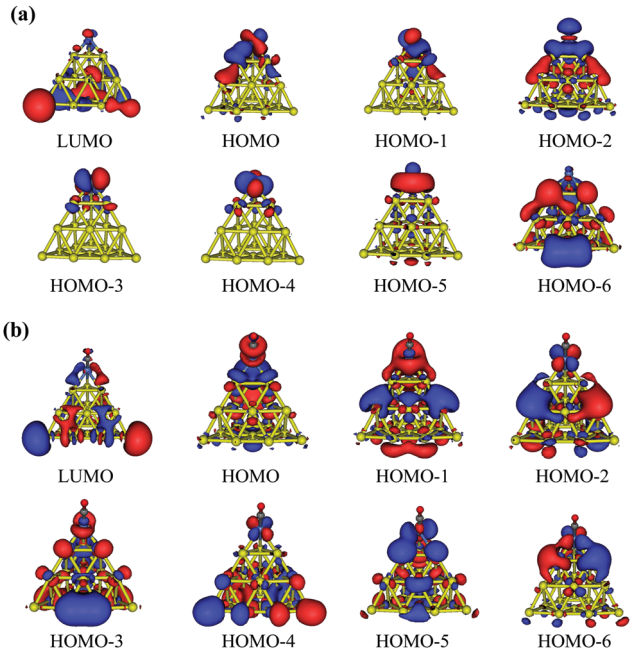

Fig. 5 The frontier molecular orbits of (a) $NiAu_{19}^-$ and (b) $[NiAu_{19}^-]$–CO.

(MOs) and density of states (DOS) of $NiAu_{19}^-$ and $[NiAu_{19}^-]$–CO structures, respectively.

Fig. 5a showed the frontier molecular orbits of the $NiAu_{19}^-$ cluster. The electron distributions of the first six filled orbitals (HOMO, HOMO−1, HOMO−2, HOMO−3, HOMO−4, HOMO−5) are mainly localized near the Ni atom. However, the electron clouds of its LUMO orbit are far away from the Ni atom, meaning that its empty valence orbits can be filled by the one lone pair electrons of the CO molecule. Such charge-flow tendencies, from ligand molecules to metal surfaces, also coincide with previous reports.[60] When a CO molecule is adsorbed on the $NiAu_{19}^-$ cluster, there are overlaps between the frontier orbitals of gold nanoalloys and the molecules. For comparison, we observe from Fig. 5b that the HOMO and HOMO−1 orbits of the $[NiAu_{19}^-]$–CO structure show the σ bonding orbit between the C and Ni atoms. The HOMO−2, HOMO−3, and HOMO−4 orbits show a back-donation interaction from the occupied d states of Ni to the unoccupied 2π MO of CO. In brief, the donation interactions still play much more important roles than back transfers, and there exist some charge flows from CO to the Ni metal.

The above observations are further confirmed by the analyses of the density of states (DOS). It is very clear in Fig. 6 that the HOMO and LUMO orbit energies change very little when a CO molecule is adsorbed on the $NiAu_{19}^-$ cluster, respectively. The $NiAu_{19}^-$ cluster has a certain contribution to the total DOS of the studied complex near the HOMO/LUMO energy level. This result reveals that the electronic structure of the $NiAu_{19}^-$ anion is not sensitive toward the CO molecule and is a good candidate for catalysis.

ETS-NOCV analysis was carried out using the Multiwfn3.8 program, which is commonly used to examine chemical bonding between fragments.[61–64] Here, the two fragments are given

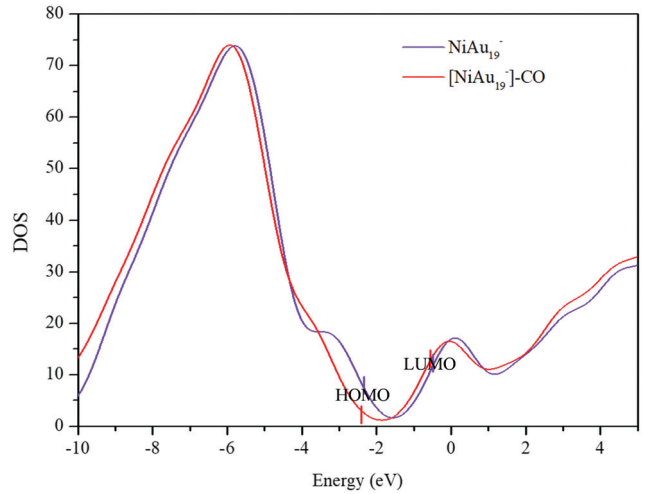

Fig. 6 The density of states of the $NiAu_{19}^-$ and $[NiAu_{19}^-]$–CO structures.

by a single CO molecule and a pyramidal cluster. From the graphs of $\Delta\rho^{Pauli}$ with large blue isosurfaces (Fig. 7), the Pauli repulsion makes the electron drop significantly in the regions between Au/Ni and CO. In contrast, there are large green areas between Au/Ni and CO in the $\Delta\rho^{Orbital}$ diagrams, reflecting a significant increase in the electron density of the bonding regions due to orbital interactions. From the perspective of the total deformation density, it is obvious that the increase in the density of the bonding area caused by the orbital interactions is higher than the decrease in the density of the bonding area caused by the Pauli repulsion. Therefore, the relationship between Au/Ni and C in the total deformation density diagram is obviously positive, presenting that the direction of charge flow in the deformation density is from CO → clusters (σ-donation).

To analyze the nature and magnitude of CO···M interactions, we considered energy decomposition analysis (EDA), which computes the interaction energy (Δ_{int}) directly *via* a perturbative approach (SAPT0), involving perturbative expansions of fluctuation and interaction potentials of the fragments.[65–67] The SAPT0 is given by $\Delta_{int} = \Delta_{elst} + \Delta_{exch} + \Delta_{ind} + \Delta_{disp}$, where Δ_{elst} is the classical electrostatic interaction term between the fragments; Δ_{exch} is the repulsive term associated with Pauli repulsion; Δ_{ind} is the inductive term; and Δ_{disp} is the term that corresponds to the long-range dispersion. Table 2 shows negative Δ_{int} values of Au_{20}–CO and $[Au_{19}Ni^-]$–CO, which are consistent with the above E_{ae} analysis results, indicating that the systems from the fragments are thermodynamically favored. A further dissection of Δ_{int} to chemically meaningful terms within the EDA shows that the nature of Au/Ni–C interactions in Au_{20}–CO and $[Au_{19}Ni^-]$–CO, with (51–62%) of electrostatic characteristics, followed by Δ_{ind} contributions (~30%) and small Δ_{disp} (<16%) contributions. Based on the results, the Au/Ni–C interactions between the fragments are dominated by Δ_{elst} (electrostatic attractions) and Δ_{ind} (orbital interactions). Moreover, the NPA charge of the selected structures was further analyzed and listed in Table S1 (ESI†). The results show that CO loses a fraction of its charge and this is

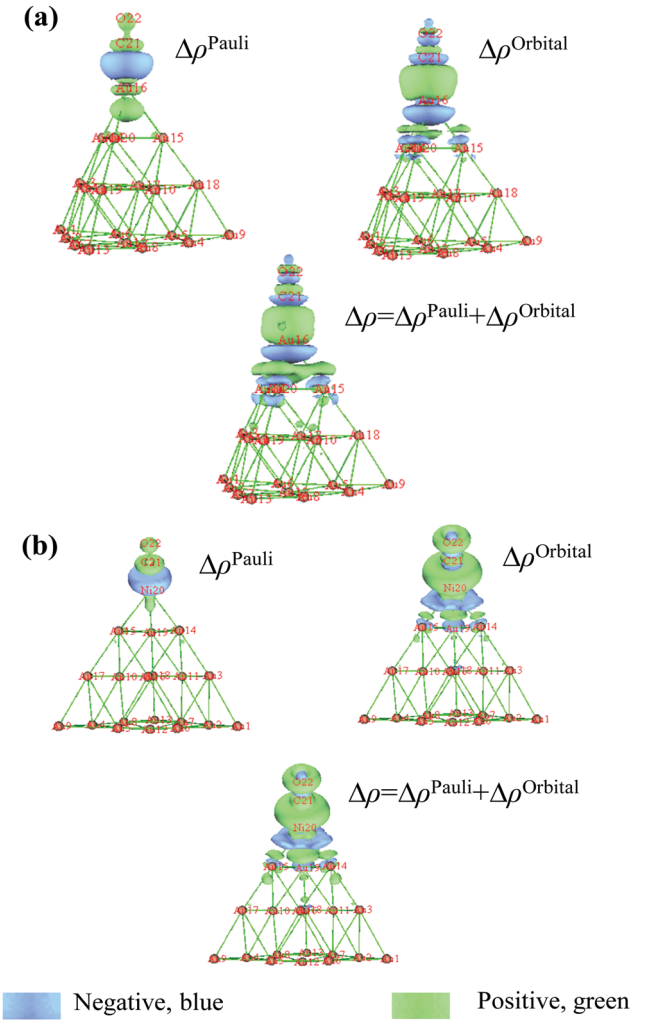

Fig. 7 The ETS-NOCV analysis of the M–CO interactions in (a) Au_{20}–CO and (b) $[NiAu_{19}^-]$–CO. The direction of charge flow in the deformation densities is from blue → green.

Table 2 Energy decomposition analysis (SAPT0) of Au_{20}–CO and $[Au_{19}Ni^-]$–CO, employing the Def2-TZVP basis set. All the values are expressed in eV except for the percentages

Systems	Δ_{int}	Δ_{elst}	Δ_{exch}	Δ_{ind}	Δ_{disp}
Au_{20}–CO	−0.72	−3.13 (51%)	5.43	−2.04 (33%)	−0.98 (16%)
$[Au_{19}Ni^-]$–CO	−1.80	−5.95 (62%)	7.91	−2.95 (30%)	−0.81 (8%)

transferred to the pyramidal clusters, which is consistent with the above ETS-NOCV analysis results, also corresponding to CO as an electron donor discussed earlier.

4. Conclusions

In summary, we investigated the structural stability, adsorption, and electronic properties of various pyramidal clusters using DFT. According to the SVB model, isoelectronic superatomic molecules with different pyramid configurations by replacing

vertex Au atoms of the pyramidal Au_{20} using metal M atoms (M = Li, Be, Ni, Cu, and Zn group atoms) are constructed. These new clusters are confirmed to be local minima on the potential energy surfaces. We further found that the adsorption of CO molecules generate very minimal changes in the parent geometries of the pyramidal clusters, and most adsorption structures are consistent with the geometry structure of CO adsorption at the vertex site of the Au_{20} cluster. The vibrational frequency analyses indicated that there are significant red shifts when CO molecules are adsorbed on the Ni/Pd/Pt atoms, where the C–O bond lengths are slightly elongated and their vibration frequencies are less than that of free CO. Moreover, the E_{ae} values of CO molecules binding with Li and Zn group atoms are relatively small (<0.5 eV), and the E_{ae} values of CO–Be are in the range of 0.5–1.0 eV. In comparison, the E_{ae} values of CO molecules binding with Ni group atoms are in the range of 1.5–2.0 eV, which are in the category of the covalent bond. The molecular orbitals and density of states reveal that there is an overlap between the frontier orbitals of the clusters and the CO molecule, and the electronic structure of $NiAu_{19}^-$ is not sensitive toward the CO molecule and is a good candidate for catalysis. ETS-NOCV analysis shows that the relationship between Au/Ni and C in the total deformation density diagram is obviously positive, showing that the direction of charge flow in the deformation densities is from CO → clusters. We also pointed out the nature and magnitude of CO–M interactions by energy decomposition analysis (from SAPT0) and NPA charge. Our work demonstrates the feasibility of the SVB model as a theoretical direction for expanding superatomic catalysts from superatom clusters.

Conflicts of interest

There are no conflicts to declare.

Acknowledgements

This work is financed by the National Natural Science Foundation of China (21873001) and the Key Project of Scientific Research Foundation of Anhui Province Education Department (KJ2021A0962). The calculations were carried out at the High-Performance Computing Center of Anhui University.

References

1 C. Cesari, J.-H. Shon and S. Zacchini, *et al.*, Metal carbonyl clusters of groups 8–10: synthesis and catalysis, *Chem. Soc. Rev.*, 2021, **50**, 9503–9539.
2 T. Imaoka, Y. Akanuma and N. Haruta, *et al.*, Platinum clusters with precise numbers of atoms for preparative-scale catalysis, *Nat. Commun.*, 2017, **8**, 1–8.
3 E. C. Tyo and S. Vajda, Catalysis by clusters with precise numbers of atoms, *Nat. Nanotechnol.*, 2015, **10**, 577–588.
4 S. Yamazoe, K. Koyasu and T. Tsukuda, Nonscalable oxidation catalysis of gold clusters, *Acc. Chem. Res.*, 2014, **47**, 816–824.
5 D. Astruc, Introduction: nanoparticles in catalysis, *Chem. Rev.*, 2020, **120**, 461–463.
6 L. Liu, M. Lopez-Haro and C. W. Lopes, *et al.*, Regioselective generation and reactivity control of subnanometric platinum clusters in zeolites for high-temperature catalysis, *Nat. Mater.*, 2019, **18**, 866–873.
7 P. Ferrari, J. Vanbuel and E. Janssens, *et al.*, Tuning the reactivity of small metal clusters by heteroatom doping, *Acc. Chem. Res.*, 2018, **51**, 3174–3182.
8 C. Dong, Y. Li and D. Cheng, *et al.*, Supported metal clusters: fabrication and application in heterogeneous catalysis, *ACS Catal.*, 2020, **10**, 11011–11045.
9 X. Ding, Z. Li and J. Yang, *et al.*, Adsorption energies of molecular oxygen on Au clusters, *J. Chem. Phys.*, 2004, **120**, 9594–9600.
10 R. Pal, L.-M. Wang and Y. Pei, *et al.*, Unraveling the mechanisms of O_2 activation by size-selected gold clusters: transition from superoxo to peroxo chemisorption, *J. Am. Chem. Soc.*, 2012, **134**, 9438–9445.
11 Z. Luo, A. Castleman Jr. and S. N. Khanna, Reactivity of metal clusters, *Chem. Rev.*, 2016, **116**, 14456–14492.
12 L. Li, Y. Gao and H. Li, *et al.*, CO oxidation on TiO_2 (110) supported subnanometer gold clusters: Size and shape effects, *J. Am. Chem. Soc.*, 2013, **135**, 19336–19346.
13 Y. Gao, N. Shao and Y. Pei, *et al.*, Icosahedral crown gold nanocluster $Au_{43}Cu_{12}$ with high catalytic activity, *Nano Lett.*, 2010, **10**, 1055–1062.
14 N. S. Khetrapal, D. Deibert and R. Pal, *et al.*, How O2-Binding Affects Structural Evolution of Medium Even-Sized Gold Clusters Au_n^-(n = 20–34), *J. Phys. Chem. Lett.*, 2021, **12**, 3560–3570.
15 J. Li, X. Zhao and Z. Ma, *et al.*, Structure and Catalytic Activity of Gold Clusters Supported on Nitrogen-Doped Graphene, *J. Phys. Chem. C*, 2021, **125**, 5006–5019.
16 Q. Wu, L. Zhou and G. C. Schatz, *et al.*, Mechanistic Insights into Photocatalyzed H_2 Dissociation on Au Clusters, *J. Am. Chem. Soc.*, 2020, **142**, 13090–13101.
17 Q. Liu, P. Fan and Y. Hu, *et al.*, Superatomic and adsorption properties of Ni atom doped Au clusters, *Phys. Chem. Chem. Phys.*, 2021, **23**, 10946–10952.
18 W. T. Wallace and R. L. Whetten, Coadsorption of CO and O_2 on selected gold clusters: Evidence for efficient room-temperature CO_2 generation, *J. Am. Chem. Soc.*, 2002, **124**, 7499–7505.
19 G.-J. Kroes, A. Gross and E.-J. Baerends, *et al.*, Quantum theory of dissociative chemisorption on metal surfaces, *Acc. Chem. Res.*, 2002, **35**, 193–200.
20 D. Borodin, I. Rahinov and P. R. Shirhatti, *et al.*, Following the microscopic pathway to adsorption through chemisorption and physisorption wells, *Science*, 2020, **369**, 1461–1465.
21 Y. Gao, N. Shao and Y. Pei, *et al.*, Catalytic activities of subnanometer gold clusters (Au_{16}–Au_{18}, Au_{20}, and Au_{27}–Au_{35}) for CO oxidation, *ACS Nano*, 2011, **5**, 7818–7829.
22 N. Nikbin, G. Mpourmpakis and D. G. Vlachos, A Combined DFT and Statistical Mechanics Study for the CO Oxidation

on the Au_{10}^{-1} Cluster, *J. Phys. Chem. C*, 2011, **115**, 20192–20200.

23 W.-L. Yim, T. Nowitzki and M. Necke, *et al.*, Universal phenomena of CO adsorption on gold surfaces with low-coordinated sites, *J. Phys. Chem. C*, 2007, **111**, 445–451.

24 W. Huang, H.-J. Zhai and L.-S. Wang, Probing the Interactions of O_2 with Small Gold Cluster Anions (Au_n^-, n = 1–7): Chemisorption vs Physisorption, *J. Am. Chem. Soc.*, 2010, **132**, 4344–4351.

25 N. Lopez, J. K. Nørskov and T. Janssens, *et al.*, The adhesion and shape of nanosized Au particles in a Au/TiO_2 catalyst, *J. Catal.*, 2004, **225**, 86–94.

26 J. Li, X. Li and H.-J. Zhai, *et al.*, Au_{20}: a tetrahedral cluster, *Science*, 2003, **299**, 864–867.

27 L. Cheng, X. Zhang and B. Jin, *et al.*, Superatom–atom superbonding in metallic clusters: a new look to the mystery of an Au_{20} pyramid, *Nanoscale*, 2014, **6**, 12440–12444.

28 A. Muñoz-Castro and R. B. King, Au_{20}. Effect of a strong tetrahedral field in a spherical concentric bonding shell model, *J. Phys. Chem. C*, 2017, **121**, 5848–5853.

29 K. Bobuatong, S. Karanjit and R. Fukuda, *et al.*, Aerobic oxidation of methanol to formic acid on Au_{20}^-: a theoretical study on the reaction mechanism, *Phys. Chem. Chem. Phys.*, 2012, **14**, 3103–3111.

30 A. Banerjee, T. K. Ghanty and A. Chakrabarti, *et al.*, Nonlinear Optical Properties of $Au_{19}M$ (M = Li, Na, K, Rb, Cs, Cu, Ag) Clusters, *J. Phys. Chem. C*, 2012, **116**, 193–200.

31 A. V. Beletskaya, D. A. Pichugina and A. F. Shestakov, *et al.*, Formation of H_2O_2 on Au_{20} and $Au_{19}Pd$ clusters: understanding the structure effect on the atomic level, *J. Phys. Chem. A*, 2013, **117**, 6817–6826.

32 K. Mondal, D. Manna and T. K. Ghanty, *et al.*, Significant modulation of CO adsorption on bimetallic $Au_{19}Li$ cluster, *Chem. Phys.*, 2014, **428**, 75–81.

33 D. Cortes-Arriagada, M. P. Oyarzún and L. Sanhueza, *et al.*, Binding of trivalent arsenic onto the tetrahedral Au_{20} and Au19Pt clusters: implications in adsorption and sensing, *J. Phys. Chem. A*, 2015, **119**, 6909–6918.

34 J. De Haeck, N. Veldeman and P. Claes, *et al.*, Carbon monoxide adsorption on silver doped gold clusters, *J. Phys. Chem. A*, 2011, **115**, 2103–2109.

35 H. T. Le, S. M. Lang and J. De Haeck, *et al.*, Carbon monoxide adsorption on neutral and cationic vanadium doped gold clusters, *Phys. Chem. Chem. Phys.*, 2012, **14**, 9350–9358.

36 Z. Luo, A. Castleman Jr. and S. N. Khanna, Reactivity of metal clusters, *Chem. Rev.*, 2016, **116**, 14456–14492.

37 T. K. Ghanty, A. Banerjee and A. Chakrabarti, Structures and the Electronic Properties of $Au_{19}X$ Clusters (X = Li, Na, K, Rb, Cs, Cu, and Ag), *J. Phys. Chem. C*, 2010, **114**, 20–27.

38 K. Mondal, A. Banerjee and T. K. Ghanty, Structural and chemical properties of subnanometer-sized bimetallic $Au_{19}Pt$ cluster, *J. Phys. Chem. C*, 2014, **118**, 11935–11945.

39 A. C. Reber and S. N. Khanna, Superatoms: electronic and geometric effects on reactivity, *Acc. Chem. Res.*, 2017, **50**, 255–263.

40 E. A. Doud, A. Voevodin and T. J. Hochuli, *et al.*, Superatoms in materials science, *Nat. Rev. Mater.*, 2020, **5**, 371–387.

41 T. Tsukamoto, T. Kambe and T. Imaoka, *et al.*, Modern cluster design based on experiment and theory, *Nat. Rev. Chem.*, 2021, **5**, 338–347.

42 D. E. Bergeron, A. W. Castleman and T. Morisato, *et al.*, Formation of $Al_{13}I^-$: Evidence for the superhalogen character of Al13, *Science*, 2004, **304**, 84–87.

43 L. Cheng and J. Yang, Communication: New insight into electronic shells of metal clusters: Analogues of simple molecules, *J. Chem. Phys.*, 2013, **138**, 141101.

44 J. P. Perdew, K. Burke and M. Ernzerhof, Generalized gradient approximation made simple, *Phys. Rev. Lett.*, 1996, **77**, 3865.

45 F. Weigend and R. Ahlrichs, Balanced basis sets of split valence, triple zeta valence and quadruple zeta valence quality for H to Rn: Design and assessment of accuracy, *Phys. Chem. Chem. Phys.*, 2005, **7**, 3297–3305.

46 J. H. Stenlid and T. Brinck, Extending the σ-hole concept to metals: An electrostatic interpretation of the effects of nanostructure in gold and platinum catalysis, *J. Am. Chem. Soc.*, 2017, **139**, 11012–11015.

47 G. W. T. M. J. Frisch, H. B. Schlegel, G. E. Scuseria, G. S. M. A. Robb, V. Barone and D. J. Fox, *G. Revision B.01, Inc.*, Wallingford CT, 2009.

48 M. U. Varetto, *Swiss National Supercomputing and M. Centre*, Switzerland, 2009.

49 T. M. Parker, L. A. Burns and R. M. Parrish, *et al.*, Levels of symmetry adapted perturbation theory (SAPT). I. Efficiency and performance for interaction energies, *J. Chem. Phys.*, 2014, **140**, 094106.

50 R. M. Parrish, L. A. Burns and D. G. Smith, *et al.*, Psi4 1.1: An open-source electronic structure program emphasizing automation, advanced libraries, and interoperability, *J. Chem. Theory Comput.*, 2017, **13**, 3185–3197.

51 B. Assadollahzadeh and P. Schwerdtfeger, A systematic search for minimum structures of small gold clusters Au_n (n = 2–20) and their electronic properties, *J. Chem. Phys.*, 2009, **131**, 064306.

52 P. Gruene, D. M. Rayner and B. Redlich, *et al.*, Structures of neutral Au_7, Au_{19}, and Au_{20} clusters in the gas phase, *Science*, 2008, **321**, 674–676.

53 H. A. Abdulhussein, P. Ferrari and J. Vanbuel, *et al.*, Altering CO binding on gold cluster cations by Pd-doping, *Nanoscale*, 2019, **11**, 16130–16141.

54 A. Fielicke, G. von Helden and G. Meijer, *et al.*, Gold cluster carbonyls: saturated adsorption of CO on gold cluster cations, vibrational spectroscopy, and implications for their structures, *J. Am. Chem. Soc.*, 2005, **127**, 8416–8423.

55 P. Ferrari, G. Libeert and N. M. Tam, *et al.*, Interaction of carbon monoxide with doped metal clusters, *CrystEngComm*, 2020, **22**, 4807–4815.

56 M. E. Tuckerman, P. J. Ungar and T. Von Rosenvinge, *et al.*, Ab initio molecular dynamics simulations, *J. Phys. Chem.*, 1996, **100**, 12878–12887.

57 Q. Liu, C. Xu and X. Wu, *et al.*, Electronic shells of a tubular Au_{26} cluster: a cage–cage superatomic molecule

based on spherical aromaticity, *Nanoscale*, 2019, **11**, 13227–13232.

58 A. Luna-Valenzuela, J. L. Cabellos and A. Posada-Amarillas, Effect of temperature on the structure of Pd_8 and Pd_7Au_1 clusters: an Ab initio molecular dynamics approach, *Theor. Chem. Acc.*, 2021, **140**, 1–10.

59 J. Hafner, Ab-initio simulations of materials using VASP: Density-functional theory and beyond, *J. Comput. Chem.*, 2008, **29**, 2044–2078.

60 X. Wu, L. Zhao and J. Jin, *et al.*, Observation of alkaline earth complexes $M(CO)_8$ (M = Ca, Sr, or Ba) that mimic transition metals, *Science*, 2018, **361**, 912–916.

61 M. P. Mitoraj, Bonding in ammonia borane: An analysis based on the natural orbitals for chemical valence and the extended transition state method (ETS-NOCV), *J. Phys. Chem. A*, 2011, **115**, 14708–14716.

62 T. Lu and F. Chen, Multiwfn: a multifunctional wavefunction analyzer, *J. Comput. Chem.*, 2012, **33**, 580–592.

63 S. Díaz, M. Z. Brela and S. Gutiérrez-Oliva, *et al.*, ETS-NOCV Decomposition of the Reaction Force: The HCN/CNH Isomerization Reaction Assisted by Water, *J. Comput. Chem.*, 2017, **38**, 2076–2087.

64 N. A. Phillips, R. Y. Kong and A. J. White, *et al.*, Group 11 Borataalkene Complexes: Models for Alkene Activation, *Angew. Chem., Int. Ed.*, 2021, **60**, 12013–12019.

65 R. V. de Amorim, K. E. Batista and G. R. Nagurniak, *et al.*, CO, NO, and SO adsorption on Ni nanoclusters: a DFT investigation, *Dalton Trans.*, 2020, **49**, 6407–6417.

66 A. F. Yonezawa, G. R. Nagurniak and R. P. Orenha, *et al.*, Stability Changes in Iridium Nanoclusters via Monoxide Adsorption: A DFT Study within the van der Waals Corrections, *J. Phys. Chem. A*, 2021, **125**, 4805–4818.

67 D. Parasar, N. B. Jayaratna and A. Muñoz-Castro, *et al.*, Carbonyl complexes of copper(I) stabilized by bridging fluorinated pyrazolates and halide ions, *Dalton Trans.*, 2019, **48**, 6358–6371.

